



Published in final edited form as:

Mol Cell Neurosci. 2019 July ; 98: 1–11. doi:10.1016/j.mcn.2019.04.002.

Klotho deficiency affects the spine morphology and network synchronization of neurons.

Hai T. Vo^a, Mary L. Phillips^a, Jeremy H. Herskowitz^b, and Gwendalyn D. King^{a,**}

^aDepartment of Neurobiology, University of Alabama at Birmingham, 1825 University Blvd. Shelby 913, Birmingham, AL, USA 35294.

^bDepartment of Neurology, University of Alabama at Birmingham 1825 University Blvd. Shelby 1114, Birmingham, AL, USA 35294.

Abstract

Klotho-deficient mice rapidly develop cognitive impairment and show some evidence of the onset of neurodegeneration. However, it is impossible to investigate the long-term consequences on the brain because of the dramatic shortening of lifespan caused by systemic klotho deficiency. As klotho expression is downregulated with advancing organismal age, understanding the mechanisms of klotho action is important for developing novel strategies to support healthy brain aging. Previously, we reported that klotho-deficient mice show enhanced long-term potentiation prior to the onset of cognitive impairment. To inform this unusual phenotype, herein, we examined neuronal structure and *in vitro* synaptic function. Our results indicate that klotho deficiency causes the population of dendritic spines to shift towards increased head diameter and decreased length consistent with mature, mushroom type spines. Multi-electrode array recordings from klotho-deficient neurons show increased synchronous firing and activity changes reflective of increased neuronal network activity. Supplementation of the neuronal growth media with recombinant shed klotho corrected some but not all of the activity changes caused by KL deficiency. Last, *in vivo* we found that klotho-deficient mice have a decreased latency to induced seizure activity. Together these data show that klotho-deficient memory impairments are underpinned by structural and functional changes that may preclude ongoing normal cognition.

Keywords

Pentylenetetrazole; aging; multi-electrode array; dendritic spine; morphology

Introduction

Aging is a complex and highly individualized process influenced by genetics and the environment. While it is clear that the risk for neurodegenerative disease increases

^{**}Corresponding author: Gwendalyn D. King, Ph.D., Department of Neurobiology, University of Alabama at Birmingham, 1825 University Blvd, Shelby 913, Birmingham, AL USA 35294, 205-996-6247 – phone, gdking@uab.edu.

Publisher's Disclaimer: This is a PDF file of an unedited manuscript that has been accepted for publication. As a service to our customers we are providing this early version of the manuscript. The manuscript will undergo copyediting, typesetting, and review of the resulting proof before it is published in its final citable form. Please note that during the production process errors may be discovered which could affect the content, and all legal disclaimers that apply to the journal pertain.

dramatically with advancing age, changes to brain structure and function occur even with non-pathological, normal brain aging (Dumitriu et al. 2010; Burke and Barnes 2006; Dickstein et al. 2013). In humans, normal brain aging is underpinned by increased or decreased expression of a relatively small percentage of genes (Lu et al. 2004) suggesting that common pathways could be targeted to better support the brain during aging. Among the genes downregulated with advancing age is α -Klotho (KL) whose protein expression is decreased in the brain with age across species (Xiao et al. 2004; Yamazaki et al. 2010; Duce et al. 2008; King et al. 2012; Semba et al. 2014). Mice genetically deficient for KL protein developed rapid onset of cognitive impairment (Nagai et al. 2003; Laszczyk et al. 2017). Likewise, humans showed that lower levels of KL correlate with the development of diseases from Alzheimer's to temporal lobe epilepsy (Teocchi et al. 2013; Semba et al. 2014). Amazingly, both genetically driven mouse KL overexpression and a polymorphism that increased circulating human KL correlated with enhanced cognition (Dubal et al. 2014; Laszczyk et al. 2017). Mice overexpressing KL are resistant to the development of neurodegenerative disease phenotypes and in the case of Alzheimer's disease models, are resistant even in the presence of pathological disease hallmarks (Dubal et al. 2015; Massó et al. 2015; Prather et al. 2015; Leon et al. 2017; Baluchnejadmojarad et al. 2017). Greater mechanistic understanding of how KL proteins influence normal brain function may allow it to be targeted to support healthy brain aging.

KL expression is limited to a few organs with the kidney and brain showing the highest expression (Kuro-o et al. 1997; Li et al. 2004; Clinton et al. 2013). KL is a transmembrane protein that can be shed from the cell surface to circulate through both serum and cerebrospinal fluid (Imura et al. 2004; Chen et al. 2007). An alternate splice variant of KL is also detected in brain (Matsumura et al. 1998; Massó et al. 2015). We showed that KL regulates hippocampal synaptic plasticity such that KL-deficient mice exhibit increased paired-pulse facilitation and long-term potentiation (LTP) while KL-overexpressing mice showed decreased LTP (Li et al. 2017). It is common for models of decreased LTP to show a concomitant decrease in cognitive performance, consistent with the idea that LTP is the molecular correlate of memory (Lu et al. 1997; Saxe et al. 2006; Lee and Silva 2009; Wang et al. 2009; Han et al. 2013). However, genetic manipulations have also produced examples that decouple LTP and cognitive performance (Kaksonen et al. 2002; Pineda et al. 2004; Niisato et al. 2005; Rutten et al. 2008; Kim et al. 2009; Migaud et al. 1998)

Herein, we sought to determine whether changes to neuronal structural or functional could provide further context to understand the relatively rare phenotype of enhanced LTP from a cognitively impaired mouse model. We tested whether KL expression alters dendritic spine morphology, affects neuronal network activity, or seizure susceptibility. Together, our data suggest KL impacts both the physical connections between neurons and neuronal activity within a network.

Materials and Methods

Animal care

All animal procedures were approved by the University of Alabama at Birmingham Institutional Animal Care and Use Committee. Systemic, constitutive KL-deficient (KO,

129S1/SvImJ) and systemic, constitutive KL-overexpressing (OE, C57BL/6J) mice were obtained from M. Kuro-o (University of Texas Southwestern). We purchased Thy1-GFP (C57BL/6J) from the Jackson Laboratory (Stock #007788; Bar Harbor, ME). All mice were allowed access to food and water *ad libitum* and housed at 26.6°C with humidity maintained at 40%. Beginning at 5-weeks of age, we supplemented KL-deficient mice with Bacon Softies or Nutra-Gel (BioServ, Frenchtown, NJ). We previously reported no effect of sex on KL-deficient mouse behavioral performance (Laszczyk et al. 2017). Herein, sex balanced groups of animals were used where possible, but sex was not determined in cultured neurons taken from P1 pups.

Dendritic spine analysis

Both image acquisition and data analysis were performed by an experimenter blind to the genotype. Imaging procedures were adapted from published protocols (Swanger et al. 2015; Greathouse et al. 2018; Boros et al. 2017). Dendritic segments were imaged using a Zeiss LSM510 laser scanning confocal microscope using a 63x oil-immersion objective with a numerical aperture of 1.4 (Zeiss, Oberkochen, Germany). Z-stack images were captured at 1024×1024 resolution with 4x line averaging, 3x zoom (pixel size of 0.041µm/pixel) and a 0.1µm Z-step interval. We imaged dendritic segments from only the apical dendrites of CA1 pyramidal neurons if they 1) were from sections ranging from bregma -1.70mm to -1.94mm representing dorsal hippocampus, 2) did not have overlapping branches from other GFP-expressing neurons, and 3) were from secondary or tertiary branches. Prior to analysis, z-stack images were deconvolved using the Huygens Software (Scientific Volume Imaging, Hilversum, Netherlands) using an automatically generated theoretical point spread function with an automatically estimated background setting. NeuronStudio software (Rodriguez et al. 2008) was utilized to trace and analyze dendritic spines and measure spine density, head diameter, and length in a semi-automated fashion by first tracing the dendritic segment and then detecting protrusions (i.e. spines) with a minimum and maximum height of 0.2 and 3.0µm, respectively. Spines were classified into 3 groups (mushroom, stubby, and thin) within NeuronStudio. The thresholds set for spine classification were the neck ratio (head diameter/neck diameter) at 1.1, the thin ratio (spine length/head diameter) at 2.5, and the mushroom size at 0.35µm. NeuronStudio software was also used to quantify functional spines by manually identifying whether GFP+ spines were apposed to Glut puncta.

Immunohistochemistry

KL lines were bred to Thy1 green fluorescent protein (GFP) mice (Feng et al. 2000). Following perfusion and 4% paraformaldehyde fixation (Sigma-Aldrich), 30µm free-floating sections were processed as described (Laszczyk et al. 2017). GFP fluorescence required no amplification for detection. However, to count presynaptic boutons, sections were incubated with anti-vesicular glutamate transporter 1 antibody (vGlut, 1:5000, Millipore: AB5905, Burlington, MA). This was detected using an Alexa 594 secondary antibody (A11076; Fisher Scientific, Waltham, MA). 4',6'-diamidino-2-phenylindole (DAPI) incubation allowed visualization of nuclei and was conducted before mounting with Prolong Gold anti-fade mounting media (Fisher Scientific).

When primary culture neurons were transfected with soluble GFP, coverslip plated neurons were fixed with 4% paraformaldehyde, endogenous peroxidases quenched with H₂O₂, and neurons permeabilized with PBS containing 0.5% TritonX-100. Following block in 5% horse serum and 0.3% TritonX-100 in PBS, cells were incubated in anti-GFP antibody (GFP, 1:500, Developmental Studies Hybridoma Bank (DSHB): 12A6, Iowa City, Iowa) overnight at 4°C. Antibody was detected using an Alexa 488 conjugated secondary antibody (A21202, Fisher Scientific) and nuclei were labeled with DAPI before mounting with Prolong Gold anti-fade mounting media.

Quantitative PCR (qPCR)

RNA was extracted and genomic DNA digested from flash frozen, freshly dissected brain or cultured neurons per manufacturer's instructions (RNAqueous Micro Total RNA isolation Kit, Fisher Scientific, AM1931). cDNA was generated using iScript RT Supermix (Biorad, Hercules, CA) per manufacturer's protocol. mRNA was measured by primer/probe duplex qPCR with SsoFast Probes Supermix containing passive ROX reference dye (Biorad). Primer/probes for mouse KL and mouse 18S ribosomal subunit were designed and synthesized by Integrated DNA Technologies (IDT, Coralville, IA). The mouse KL primer/probe mix contained the following sequences – Probe: 5'–/56–FAM/ATGGACGGT/ZEN/TTCGAGTGGCATAGG/3IABkFQ/–3', Primer 1: 5'–CTCAGAAAGTCAACGTAGAAGAGT–3', Primer 2: 5'–CTCAAGAAGTTCATAATGGAAACCT–3'. The mouse 18S primer/probe mix contain the following sequences – Probe: 5'–/5HEX/ACCGATTGG/ZEN/ATGGTTTATGAGGCC/3IABkFQ/–3', Primer 1: 5'–ATAGTCAAGTTCGACCGTCTTC–3', Primer 2: 5'–GTTGATTAAGTCCCTGCCCTT–3'. qPCR was performed on a StepOne qPCR system (Applied Biosystems, Foster City, CA). Fold change relative to wild-type brain or wild-type culture was calculated using the Ct method (Clinton et al. 2013).

Western Blot

Hippocampal or primary neuronal culture lysates were prepared by homogenizing in RIPA buffer containing protease inhibitors. Following BCA assay (Fisher Scientific), we separated 20–60µg of lysate through 10% polyacrylamide gels and transferred protein to nitrocellulose membranes (Fisher Scientific). Membranes were blocked with 5% non-fat dry milk in Tris-buffered saline with 0.1% Tween 20 (TBST). Membranes were incubated in primary antibody (in 0.3% BSA in TBST) at 4°C overnight using antibodies to detect KL (KL2–34, 1:200 (Maltare et al. 2014)), β-tubulin (1:10,000, DSHB, E7), synaptophysin (1:10,000, Abcam, AB52636, Cambridge, MA), GABA(A) α1 receptor (1:5000, Alomone labs, aga–001, Jerusalem, Israel), GluN1 (1:500, Neuromab, 75–272, Davis, CA), GluN2b (1:1000, Millipore, 06–600, Billerica, MA), GluR1 (1:500, Santa Cruz, sc55509, Dallas, TX), GluR2 (1:500, Neuromab, 75–002), PSD–95 (1:500, Abcam, ab18258, Cambridge, MA), v-Glut (1:500, Neuromab, 73–006) and His Tag (1:1000, Fisher Scientific, MA1–21315). Secondary antibodies conjugated to HRP were detected by chemiluminescence (Immobilon, Millipore or Supersignal, Fisher Scientific) and exposure to film. Band intensity was quantified using Image J (Schneider et al. 2012).

Synaptic membrane preparation

Synaptic membranes were prepared as described (Li et al. 2017; Goebel-Goody et al. 2009; Dubal et al. 2014). Hippocampi were homogenized with a Teflon-coated pestle in sucrose buffer (320mM sucrose, 10mM Tris, pH 7.5, 1mM Na₃VO₄, 5mM NaF, 1mM EDTA and 1mM EGTA), centrifuged at 1,000xg and then the resulting supernatant at 10,000xg. The pellet was homogenized in a limited volume of sucrose buffer and then gently rotated in 8 volumes of pellet buffer (0.5% Triton X100, 10mM Tris pH 7.5, 1mM Na₃VO₄, 5mM NaF, 1mM EDTA and 1mM EGTA) before centrifugation at 32,000xg. The post-synaptic density, localized to the pellet was resuspended by sonication in resuspension buffer (1% SDS, 10mM Tris pH 7.5, 1mM Na₃VO₄, 5mM NaF, 1mM EDTA and 1mM EGTA with 1X Halt protease inhibitor cocktail (78430, Fisher Scientific). Presynaptic proteins in the supernatant were acetone concentrated overnight, separated from acetone, and resuspended by sonication into resuspension buffer with 1X Halt protease inhibitor cocktail. Fractions were processed for Western blot.

Primary Neuronal Culture

Genotyping of postnatal pups (P0–P1) was determined by rapid DNA extraction and genotyping per manufacturer's instructions (Terra PCR Direct Genotyping Kit; Takara Bio, Kusatsu, Japan). Brains of the same genotype were pooled for processing when possible. Hippocampal neurons were isolated using an adapted protocol (Beaudoin et al. 2012). Briefly, hippocampi were isolated in dissection media containing 0.1% sucrose, 10mM HEPES, and 0.11mg/mL sodium pyruvate in Ca²⁺ and Mg²⁺ free HBSS (GE Healthcare Life Sciences, Marlborough, MA). Tissue was dissociated by incubation in papain and DNase (Worthington, Lakewood, NJ) dissolved in HBSS for 20 minutes at 37°C. Cells were further dissociated mechanically with flame-polished glass Pasteur pipettes before plating on 0.05% polyethylenimine (PEI; Sigma-Aldrich) coated tissue culture plates for biochemical assays. Glass coverslips (Fisher Scientific) and multi-electrode arrays (MEA60-200-30-3D; Qwane, Lausanne, Switzerland) were coated with PEI and mouse laminin (20µg/mL; Corning, Corning, NY). We maintained neurons in Neurobasal media containing B27 supplement (Fisher Scientific) and 2mM L-glutamine (GE Healthcare Life Sciences) with half media changes every 2–3 days. 5µM of AraC (Sigma-Aldrich) was added to maintenance media at the first media change. When used, bioactive recombinant mouse KL (100ng/mL; 1819-KL-050; R&D Systems, Minneapolis, MN) (Leon et al. 2017; Vadakke Madathil et al. 2014; Lim et al. 2017; Laszczyk et al. 2017) was diluted and added to culture media at the first media change and each interval thereafter. Recombinant KL is supplied in PBS with 50% glycerol and 0.1 mM EDTA and diluent was mimicked in control conditions.

For *in vitro* spine analysis, neurons were transfected with soluble GFP plasmid (Xu and Pozzo–Miller 2017; Xu et al. 2017) using Lipofectamine 2000, per manufacturer's instructions (Fisher Scientific) diluted in Neurobasal media.

Multi-electrode array electrophysiology

The multi-electrode arrays (MEA) have 30µm diameter electrodes with 200µm inter-electrode distance aligned to an 8×8 grid (Qwane). We recorded activity using the MEA-60-System amplifier and MC_Rack software (Multi Channel Systems, Reutlingen, Germany).

When wild-type and KL-deficient neurons were tested, recordings were filtered using a high-pass 2nd Order Butterworth filter with a 200Hz cutoff frequency and a $-20\mu\text{V}$ threshold set for spike detection. When the effects of recombinant KL were tested, recordings were filtered with a high-pass 2nd Order Butterworth filter with a 300Hz cutoff frequency and a threshold set for spikes detection that was variable dependent on noise from the ground electrode. These thresholds were reached after determining the amplitude of noise recorded on the ground electrode, analyzing waveforms of identified spikes using the different μV cutoffs, and analyzing the consistency of baseline recordings with different cutoffs. The cutoffs were only mildly conservative, resulting in a false detection rate of roughly 0.07–0.1Hz on the ground electrode to avoid filtering out true spikes on other channels. Cutoff frequencies were not significantly different between groups or time points.

To chronically increase network activity, $10\mu\text{M}$ bicuculline (Enzo Life Sciences, Farmingdale, New York) was added to the maintenance media. We performed one-minute recordings on day 11–13 *in vitro* measuring at baseline, 0.5, 9, 24, and 48 hours after bicuculline supplementation. Spike detection protocols and recording time points were adapted from previously described protocols (Lu et al. 2016; Bateup et al. 2013; Yu et al. 2018). Data was analyzed using custom MATLAB scripts. All MATLAB code is available by request. Briefly, electrodes were excluded if they had fewer than 10 spikes in 60 seconds (Zhang et al. 2009) or if 75% of the firing frequency was over 5Hz, indicative of noise contamination. We used MEAs with 15–20 electrodes that met these criteria. Synchronous events were found by combining all spike activity within an MEA, binning the spikes (0.2 second bins), and finding peaks of bins that had greater than 1% of all spikes. A correlation r value was calculated by using spike timestamps and determining the correlation of each electrode to every other electrode within an MEA (MATLAB function: `xcorr`). We used the maximum absolute value for each electrode. MEA statistics were calculated by flattening all spike timestamps within an MEA. Bursts were detected with an inter-spike interval threshold of 0.008 seconds. For time series experiments, electrodes were only included if they met the previously defined criteria for all time points. Spikes per electrode over bicuculline treatment were normalized to their baseline values. Synchronous events were not normalized because some MEAs reported no synchronous events at baseline. We excluded individual values if they were determined to be statistical outliers by Robust regression and Outlier removal testing at 0.1%.

Pentylentetrazole challenge

We administered pentylentetrazole (PTZ; Sigma–Aldrich, St. Louis, MO) at 60mg/kg by a single intraperitoneal injection. Immediately thereafter, we observed mice for 20 minutes with simultaneous video recording. Although observers were blind to genotype, KL-deficient mice are markedly smaller than controls. To control for potential bias, mice were coded to prevent association by mouse line and groups of mice from various genetic lines were run in large cohorts to further prevent bias. The time to first occurrence of a phenotype/stage of seizure severity was scored as follows: 0 - normal behavior, 1 – immobility/freezing, 2 – generalized spasm, tremble or twitch, 3 – tail extension to 90 degrees, 4 – forelimb clonus, 5 – generalized clonic activity, 6 – bouncing/running seizure, 7 – full tonic extension, 8 – death (Roberson et al. 2007; Roberson et al. 2011).

Statistics

Statistical analysis was performed using GraphPad Prism software (Prism version 7.03; GraphPad, La Jolla, CA). Statistical significance is indicated as a p -value less than 0.05. For *in vivo* spine analysis, an animal is considered a sample and $n=3$ for wild-type (129S1)/KL-deficient and wild-type (C57B6)/KL overexpressor comparisons. Overall, 5314 μm of dendrite and 13,488 spines were analyzed (wild-type (129S1) = 1260 μm dendrite length/2912 spines; KL-deficient = 1245/2859; wild-type (C57B6) = 1118/2581; and KL overexpressor = 1691/5136). For *in vitro* spine analysis, a neuron was considered a sample and $n=14$ for wild-type and $n=12$ for KL-deficient cultures. Overall, 1,291 μm of dendrite and 1,668 spines were analyzed (wild-type = 658 μm dendrite length/833 spines; KL-deficient = 634/835). For MEA analysis, a sample definition differed based on the analysis. Each electrode was considered a sample when measuring the number of spikes per electrode ($n=47$ electrodes for wild-type and KL-deficient), each MEA a sample for synchronous events ($n=5$ wild-type, 4 KL-deficient MEAs), each spike a sample for spike correlation ($n=725$ wild-type, 1071 KL-deficient spikes), each burst a sample for inter-spike interval (ISI; $n=283$ wild-type, $n=122$ KL-deficient bursts), each electrode a sample for spikes per burst over time ($n=47$ electrodes for wild-type and KL-deficient), and each MEA a sample for synchronous events over time ($n=5$ wild-type, 4 KL-deficient MEAs). When the effect of recombinant KL (rKL) was tested, $n=78$ KL-deficient control and $n=71$ KL-deficient with rKL electrodes for spikes per electrode; $n=13$ KL-deficient control and $n=9$ KL-deficient with rKL MEAs for synchronous events; $n=764$ KL-deficient control and $n=623$ KL-deficient with rKL spikes for spike correlation; $n=231$ KL-deficient control and $n=94$ KL-deficient with rKL bursts for ISI; and $n=236$ KL-deficient control and $n=94$ KL-deficient with rKL bursts for spikes per burst.

Mann–Whitney tests were used for baseline MEA measures and two-way ANOVA with Sidak multiple comparisons was used when the effect of bicuculline over time was measured. Elsewhere, the normality of data sets was tested using the D’Agostino–Pearson normality test. Data sets that were not normally distributed were compared by Mann–Whitney test and normal data by Student’s t -test, ANOVA, or two-sample Kolmogorov–Smirnov test as indicated in figure legends.

Results and Discussion

Klotho deficiency alters hippocampal dendritic spine morphology.

Since KL-deficient mice show enhanced synaptic plasticity (Li et al. 2017), we sought to determine whether KL-deficiency also affected neuronal structure. Dendritic spines are actin rich protrusions along a neuronal dendrite where synaptic connections occur and information is passed between neurons. Synaptic activity influences the number and shape of spines from early neuronal development to aging (Alvarez and Sabatini 2007; Holtmaat and Svoboda 2009; Kasai et al. 2010). Synaptic strength and activity are inseparably linked to the ability of spines to undergo cytoplasmic remodeling (Hayashi and Majewska 2005). Previous data reported that KL deficiency causes decreased spine density as total synaptophysin and the number of synaptophysin puncta were reduced (Shiozaki et al. 2008; Li et al. 2004). Because of our previous result of increased LTP, we were interested in post-synaptic spine

morphology. We crossed KL-deficient mice to Thy1–GFP mosaic mice to generate mice that stochastically express GFP across the extent of mature neurons (Feng et al. 2000). This allowed us to visualize and measure dendritic spines from secondary and tertiary branches of apical dendrites of hippocampal CA1 neurons (Figure 1A). At seven weeks of age, the age when KL-deficient mice are cognitively impaired (Nagai et al. 2003; Laszczyk et al. 2017), we measure no changes to spine density or the ratio of functional spines (GFP+ spine directly apposed to a presynaptic terminal labeled by vGlut immunostain) (Figure 1A–E). To determine if spine morphology might explain the discrepancy with the previous report of fewer pre-synaptic proteins/puncta (Shiozaki et al. 2008; Li et al. 2004), we quantified the number of spines fitting into the classic morphology categories of mushroom, stubby, or thin (Hering and Sheng 2001; Harris et al. 1992; Hayashi and Majewska 2005). KL-deficient mice show fewer thin spines and a concomitant but not statistically significant increase in mushroom spines (Figure 1F). Further analyses revealed that KL-deficient spines have larger head diameters and shorter spine lengths across the spine population (Figure 1G–J). This suggests a population shift toward more structurally stable, mushroom spines but fewer thin, dynamic spines (Boros et al. 2019; Boros et al. 2017). The shortened lifespan of these mice prevents determining whether spine loss would occur given a longer life without KL, as is observed in non-human primate models of cognitive aging (Uemura 1980; Dickstein et al. 2013; Duan et al. 2003; Dumitriu et al. 2010; Page et al. 2002). While we did not see the decreased spine density that is a hallmark of older brains, we did observe selective loss of thin spines reported to correlate with cognitive impairment in aging models (Dumitriu et al. 2010; Xu et al. 2018). This could suggest the possibility that the normal age-related downregulation of KL across species could affect the structural plasticity of neurons.

Klotho deficiency increases *in vitro* neuronal network activity after stimulation.

Our previous report showed enhanced paired-pulse facilitation and enhanced LTP prior to the onset of cognitive impairment (Li et al. 2017). Together with our new data showing KL deficiency resulting in spines with increased head size and decreased length, these could indicate an impact on neuronal network activity. To test this possibility, we cultured KL-deficient hippocampal neurons from postnatal day 1 pups to observe the effects of KL deficiency on neurons and neuronal networks in culture. KL-deficient mice show significantly reduced KL protein and mRNA as do neurons isolated from KL-deficient pups (Figure 1K,L). As well, cultured KL-deficient neuronal spine morphology was similar to *in vivo* observations showing *in vitro* increased spine head diameter (Figure 1M,N). With this, we cultured neurons on 60-electrode multi-electrode arrays (MEAs) to allow recording and analysis of the effects of KL on the activity of neurons and neuronal networks (Figure 2 A–C). At baseline, we found that KL-deficient neurons have decreased activity as measured by the number of spikes per electrode (Figure 2D). Despite this decrease, across the MEA electrodes, KL-deficient neurons exhibit a significant increase in the number of synchronous events as each spike had a greater predictive value for spiking at other electrodes (Figure 2E,F). This increase in correlation altered the bursting characteristics across the MEAs such that the inter-spike interval is significantly reduced within bursts (Figure 2G) while the number of spikes within a burst is not changed (Figure 2H). These data indicate that the number of events that occur within a given burst occur at a significantly shorter interval in

KL-deficient neurons. These data suggest that at baseline, *in vitro*, spontaneous activity of KL-deficient neurons is altered.

To determine how the enhanced correlated activity of KL-deficient neurons affects the response of their neuronal networks to perturbation of network activity; we added the GABA_A receptor antagonist bicuculline to culture media simulating chronically increased neuronal activity (Figure 2A–C,I,J). We performed one-minute recordings at 0.5, 9, 24 and 48 hours after bicuculline supplementation. As expected, both wild-type and KL-deficient neurons responded to bicuculline by increasing activity as measured by the numbers of spikes per electrode and numbers of synchronous events from 0.5 to 24 hours (Figure 2I,J). As part of the neuronal homeostatic downscaling response, neurons under conditions of chronically increased activity restore baseline firing (Bateup et al. 2013). Consistently, both wild-type and KL-deficient neurons return to baseline firing by 48 hours of consistent bicuculline supplementation (Figure 2I,J). Of note, the KL-deficient neurons show a significantly greater number of synchronous events at 24 hours than wild-type (Figure 2J). These data suggest that, at least *in vitro*, KL deficiency increases the network response of neurons. When considered with spine morphology *in vivo*, MEA results could represent a hyper-connected network mediated by dendritic spines with shorter lengths and larger head diameters (Figure 1 and Figure 2A, B) that can more readily respond to stimuli (Matsuzaki et al. 2001; Zito et al. 2009; Mattison et al. 2014).

Although measures from *in vitro* culture systems require confirmation of physiological relevance, our *in vitro* data support the idea that KL deficiency may increase connectivity of neuronal networks which is consistent with previous data reporting that KL-deficient mice have increased responses to high-frequency stimulation (Li et al. 2017). Increased circuit activity can impinge on the ability of the hippocampus to encode memories. When hippocampal LTP is saturated by high-frequency stimulation *in vivo*, memory formation is impaired (Moser et al. 1998; Castro et al. 1989; McNaughton et al. 1986) suggesting the need for specificity of potentiation at certain synapses to encode memory. This specificity cannot be reached when the network response is generally increased and thus impairments in memory can result, as is seen in KL-deficient mice (Nagai et al. 2003; Laszczyk et al. 2017). Reports showing the link between increased activity, specifically LTP, and impaired memory formation are rare but seen with mutations in proteins involved in synaptic function that have a variety of roles including protein phosphorylation and scaffolding (Migaud et al. 1998; Uetani et al. 2000; Pineda et al. 2004; Rutten et al. 2008; Kim et al. 2009). Furthermore, the observation that cultured KL-deficient neurons might have a prolonged downscaling response to bicuculline (Figure 2I) could provide initial evidence of KL deficiency affecting the efficacy of the post-synapse through regulation of homeostatic downscaling (Sun and Turrigiano 2011). Additionally, increased synchronous firing within neuronal networks can be driven by a variety of factors including abnormal development and altered intrinsic excitability (Chen et al. 2006; Penn et al. 2016; van Pelt et al. 2004). Whether the KL-deficient neuron effect we measure (Figure 2) is a deficit in homeostatic downscaling or, rather, is a result of the increased synchronous activity in response to bicuculline remains to be fully determined.

To determine whether KL-deficient spine morphology and activity-related changes are the result of altered synaptic protein expression, we measured total abundance of a panel of synaptic proteins. Lysates from cultured neurons showed no differences in synaptic protein abundance (Figure 2K). With the some biological variation in lysates derived from cultured neurons, we also measured synaptic protein abundance in hippocampal lysates and again found no differences between WT and KL-deficient neurons (Figure 2K,L). Moreover, fractionation of synaptic membranes show no change in a panel of ionotropic glutamate receptors (Figure 2M). With many synaptic proteins showing normal expression level, synaptic protein function or function of downstream proteins may be the mechanism by which KL affects morphology and function of synapses.

Shed KL reduces bursting kinetics across cultured neuronal networks.

The brain is reported to host all forms of KL protein: transmembrane, shed, and secreted (Shiraki-Iida et al. 1998; Matsumura et al. 1998; Imura et al. 2004; Massó et al. 2015; Massó et al. 2017). Although short term incubation of slice cultures with shed KL did not affect synaptic transmission (Li et al. 2017), shed KL did correct neural stem cell proliferation deficits (Laszczyk et al. 2017). Increasing evidence suggests that extracellular forms of KL can influence brain function both within the central nervous system and from peripheral signaling (Leon et al. 2017; Massó et al. 2017). Although we do not fully understand KL proteins' function sufficient to attribute specific brain phenotypes to one or more forms, cerebrospinal fluid circulation of extracellular KL proteins (Imura et al. 2004; Semba et al. 2014; Kunert et al. 2017) could allow broad effects of KL upon neurons. To see if shed KL could affect baseline neuronal network activity, KL-deficient neurons were supplemented with 100ng/mL of recombinant mouse shed KL for the two weeks prior to MEA recording (Figure 3A). While we found no change in the synchronicity or correlation of events (Figure 3C,D), we measured an overall decrease in the number of spikes per electrode with recombinant KL supplementation (Figure 3B). Additionally, we found an increase in inter-spike interval within bursts and a decrease in the number of spikes per burst with recombinant KL supplementation (Figure 3E,F). These data suggest that while recombinant shed KL does not reverse all MEA measured effects of KL deficiency; it does decrease activity and reduce bursting kinetics.

The concentration of recombinant shed KL used in these experiments is higher than reported of human physiological shed KL (Kunert et al. 2017; Yamazaki et al. 2010; Imura et al. 2004; Koyama et al. 2015). Notably, although recombinant KL is reportedly bioactive (Leon et al. 2017; Vadakke Madathil et al. 2014; Lim et al. 2017; Laszczyk et al. 2017) it may not completely represent endogenous shed KL activity. Thus, results from our studies, while representative, likely underestimates shed KL function *in vivo*. Nevertheless, the modest effects seen with the chronic supplementation of shed recombinant KL might suggest either a more prominent role of transmembrane KL or synergistic roles for both transmembrane and shed KL in regulating neuronal activity.

Klotho deficiency increases seizure susceptibility.

Although it is unclear whether a cause or consequence, epileptic patient brains show changes in spine density and morphology (Wong and Guo 2013). Humans with temporal lobe

epilepsy also show decreased expression of hippocampal KL mRNA, however, it is unclear if or how KL is involved in human seizure pathology (Teocchi et al. 2013). KL-deficient mice show no evidence of the common epileptic pathology of hippocampal sclerosis (Laszczyk et al. 2017); however, their shortened lifespan, may prevent full appreciation of KL-deficient brain effects (Kuro-o et al. 1997). To test if altered synaptic morphology and increased network synchrony (Figure 1,2) could affect seizure susceptibility, we chemically induced seizures *in vivo* using the pentylenetetrazole (PTZ) seizure model of generalized tonic-clonic seizure (Roberson et al. 2011; Roberson et al. 2007; Löscher and Nolting 1991; Löscher et al. 1991). As seizure susceptibility is highly individualized, not all wild-type mice reach generalized seizure stage (Löscher et al. 1991). Consistent with this, by 20 minutes post-PTZ injection, most but not all of our wild-type mice reach a generalized seizure stage (Figure 4A,B). Mice with half the normal levels of KL (KL-deficient heterozygous mice, Het) were not significantly different from wild-type mice (Figure 4A,B). However, all KL-deficient mice reached the generalized seizure stage and did so with significantly decreased latency (Figure 4A,B). Thus, total KL deficiency increases seizure susceptibility.

Klotho overexpression does not affect seizure susceptibility but alters spine morphology.

KL overexpression increased cognitive function and prevented development of neurodegenerative diseases in mouse models of disease (Dubal et al. 2014; Dubal et al. 2015). Since constitutive overexpression increases both transmembrane and shed KL it is not currently possible to determine which form of KL protein mediate these effects. As well, although neurons express KL and fractionation showed post-synaptic compartment localization of KL protein, KL overexpressing mice do not have elevated transmembrane KL in the post-synapse (Li et al. 2017). KL-overexpressing mice show the most dramatic effects of KL overexpression after ~6 months of age (Laszczyk et al. 2017; Dubal et al. 2014; Krick et al. 2018). Since neurons isolated from P1 pups are unlikely to model physiology changes that take at least 6 months to develop, we did not culture KL-overexpressing neurons. However, we did examine seizure susceptibility, at the age when cognitive effects are well documented (Laszczyk et al. 2017; Dubal et al. 2014). 6-month-old KL-overexpressing mice showed no seizure susceptibility difference (Figure 4C,D) suggesting that increasing KL above wild-type levels does not provide a protective effect in this model.

KL-overexpression is reported to not alter synaptic density when measuring the total number of spinophilin, a protein localized to the post-synapse of dendritic spines (Sarrouilhe et al. 2006), positive puncta (Dubal et al. 2015). When we use KL-overexpressing mice expressing Thy1-GFP, we found increased spine density but without changing the functional spine ratio (Figure 5A-F). When we classified spine morphology, we found an increased number of thin spines (Figure 5G). Consistently, spines from KL-overexpressing mice exhibit smaller head diameters and increased length (Figure 5H-K). As with the KL-deficient mice, KL-overexpressing mice revealed a structural phenotype that is consistent with their cognitive status (Nagai et al. 2003; Laszczyk et al. 2017; Dubal et al. 2014). The spine population shift to include more spines with smaller head diameter and increased length may suggest greater potential for structural plasticity, as these spines may be consistent with thin, “learning

spines” that are more structurally labile and are thus more conducive to memory formation (Kasai et al. 2010; Kasai et al. 2003).

Conclusion

Herein we show that *in vivo*, systemic KL deficiency increases hippocampal neuron spine head diameter and shortens spine length (Figure 1) but see the inverse with systemic KL-overexpressing neurons. Thus, we provide the first evidence that KL expression affects dendritic spine morphology. KL-deficient neurons cultured on MEA plates show how changes to spine morphology might functionally alter neuronal networks, most notably increasing synchronous firing at baseline and under conditions stimulating high neuronal activity (Figure 2). Increased KL-deficient mouse susceptibility to induced seizure activity (Figure 4) may suggest that the effects we measured *in vitro*, are relevant to normal brain function. These new data complement our previous report where KL-deficient hippocampal slices show increased LTP (Li et al. 2017). Mice with similar electrophysiological signatures occur when the function of the post-synapse is impaired (Uetani et al. 2000; Migaud et al. 1998). This shared phenotype with impaired post-synaptic protein function and KL-deficient mice may point towards a role for a KL in post-synaptic structure or function. Further investigation into KL function in and on the post-synapse is required to determine the KL molecular mechanisms of action. Likewise, additional studies are required to distinguish how transmembrane, shed, and secreted KL proteins function individually and together to affect neuronal and thus brain function.

Acknowledgements

We deeply appreciate thoughtful discussion and support provided by Lucas Pozzo–Miller, Ph.D., University of Alabama at Birmingham and thank Melissa Garcia, University of Alabama at Birmingham, for her technical assistance with PTZ assays.

Funding Sources

Work was funded in part by the National Institutes of Health (NIA R56AG052936; GDK) and Civitan International Emerging Scholar Award (HTV).

Abbreviations

DAPI	4',6-diamidino-2-phenylindole
BCA	bicinchoninic acid assay
cDNA	complement deoxynucleic acid
DNA	deoxynucleic acid
EDTA	Ethylenediaminetetraacetic acid
FGF-23	fibroblast growth factor 23
rKL	recombinant mouse klotho
GFP	green fluorescent protein

HBSS	Hank's Balanced Salt Solution
HEPES	4-(2-hydroxyethyl)-1-piperazineethanesulfonic acid
Het	Heterozygote
KL	Klotho
OE	Klotho-overexpression mouse
KO	Klotho-deficient mouse
LTP	long-term potentiation
mRNA	messenger RNA
MEA	multi-electrode array
PBS	Phosphate buffered saline
PTZ	pentylentetrazole
qPCR	quantitative polymerase chain reaction
RIPA	radioimmunoprecipitation assay
RNA	ribonucleic acid
S.E.M	standard error of the mean
TBST	Tris-buffered saline with Tween-20
vGlut	vesicular glutamate transporter

References

- Alvarez VA and Sabatini BL 2007 Anatomical and physiological plasticity of dendritic spines. *Annual Review of Neuroscience* 30, pp. 79–97.
- Baluchnejadmojarad T, Eftekhari S-M, Jamali-Raeufy N, Haghani S, Zeinali H and Roghani M 2017 The anti-aging protein klotho alleviates injury of nigrostriatal dopaminergic pathway in 6-hydroxydopamine rat model of Parkinson's disease: Involvement of PKA/CaMKII/CREB signaling. *Experimental Gerontology* 100, pp. 70–76. [PubMed: 29107062]
- Bateup HS, Deneffrio CL, Johnson CA, Saulnier JL and Sabatini BL 2013 Temporal dynamics of a homeostatic pathway controlling neural network activity. *Frontiers in Molecular Neuroscience* 6, p. 28. [PubMed: 24065881]
- Beaudoin GMJ, Lee S-H, Singh D, Yuan Y, Ng Y-G, Reichardt LF and Arikath J 2012 Culturing pyramidal neurons from the early postnatal mouse hippocampus and cortex. *Nature Protocols* 7(9), pp. 1741–1754. [PubMed: 22936216]
- Boros BD, Greathouse KM, Gearing M and Herskowitz JH 2019 Dendritic spine remodeling accompanies Alzheimer's disease pathology and genetic susceptibility in cognitively normal aging. *Neurobiology of Aging* 73, pp. 92–103. [PubMed: 30339964]
- Boros BD, Greathouse KM, Gentry EG, Curtis KA, Birchall EL, Gearing M and Herskowitz JH 2017 Dendritic spines provide cognitive resilience against Alzheimer's disease. *Annals of Neurology* 82(4), pp. 602–614. [PubMed: 28921611]
- Burke SN and Barnes CA 2006 Neural plasticity in the ageing brain. *Nature Reviews. Neuroscience* 7(1), pp. 30–40. [PubMed: 16371948]

- Castro CA, Silbert LH, McNaughton BL and Barnes CA 1989 Recovery of spatial learning deficits after decay of electrically induced synaptic enhancement in the hippocampus. *Nature* 342(6249), pp. 545–548. [PubMed: 2586626]
- Chen C, Chen L, Lin Y, Zeng S and Luo Q 2006 The origin of spontaneous synchronized burst in cultured neuronal networks based on multi-electrode arrays. *Bio Systems* 85(2), pp. 137–143.
- Chen C-D, Podvin S, Gillespie E, Leeman SE and Abraham CR 2007 Insulin stimulates the cleavage and release of the extracellular domain of Klotho by ADAM10 and ADAM17. *Proceedings of the National Academy of Sciences of the United States of America* 104(50), pp. 19796–19801. [PubMed: 18056631]
- Clinton SM, Glover ME, Maltare A, Laszczyk AM, Mehi SJ, Simmons RK and King GD 2013 Expression of klotho mRNA and protein in rat brain parenchyma from early postnatal development into adulthood. *Brain Research* 1527, pp. 1–14. [PubMed: 23838326]
- Dickstein DL, Weaver CM, Luebke JI and Hof PR 2013 Dendritic spine changes associated with normal aging. *Neuroscience* 251, pp. 21–32. [PubMed: 23069756]
- Duan H, Wearne SL, Rocher AB, Macedo A, Morrison JH and Hof PR 2003 Age-related dendritic and spine changes in corticocortically projecting neurons in macaque monkeys. *Cerebral Cortex* 13(9), pp. 950–961. [PubMed: 12902394]
- Dubal DB, Yokoyama JS, Zhu L, Broestl L, Worden K, Wang D, Sturm VE, Kim D, Klein E, Yu G-Q, Ho K, Eilertson KE, Yu L, Kuro-o M, De Jager PL, Coppola G, Small GW, Bennett DA, Kramer JH, Abraham CR, Miller BL and Mucke L 2014 Life extension factor klotho enhances cognition. *Cell reports* 7(4), pp. 1065–1076. [PubMed: 24813892]
- Dubal DB, Zhu L, Sanchez PE, Worden K, Broestl L, Johnson E, Ho K, Yu G-Q, Kim D, Betourne A, Kuro-O M, Masliah E, Abraham CR and Mucke L 2015 Life extension factor klotho prevents mortality and enhances cognition in hAPP transgenic mice. *The Journal of Neuroscience* 35(6), pp. 2358–2371. [PubMed: 25673831]
- Duce JA, Podvin S, Hollander W, Kipling D, Rosene DL and Abraham CR 2008 Gene profile analysis implicates Klotho as an important contributor to aging changes in brain white matter of the rhesus monkey. *Glia* 56(1), pp. 106–117. [PubMed: 17963266]
- Dumitriu D, Hao J, Hara Y, Kaufmann J, Janssen WGM, Lou W, Rapp PR and Morrison JH 2010 Selective changes in thin spine density and morphology in monkey prefrontal cortex correlate with aging-related cognitive impairment. *The Journal of Neuroscience* 30(22), pp. 7507–7515. [PubMed: 20519525]
- Feng G, Mellor RH, Bernstein M, Keller-Peck C, Nguyen QT, Wallace M, Nerbonne JM, Lichtman JW and Sanes JR 2000 Imaging neuronal subsets in transgenic mice expressing multiple spectral variants of GFP. *Neuron* 28(1), pp. 41–51. [PubMed: 11086982]
- Goebel-Goody SM, Davies KD, Alvestad Linger RM, Freund RK and Browning MD 2009 Phosphoregulation of synaptic and extrasynaptic N-methyl-d-aspartate receptors in adult hippocampal slices. *Neuroscience* 158(4), pp. 1446–1459. [PubMed: 19041929]
- Greathouse KM, Boros BD, Deslauriers JF, Henderson BW, Curtis KA, Gentry EG and Herskowitz JH 2018 Distinct and complementary functions of rho kinase isoforms ROCK1 and ROCK2 in prefrontal cortex structural plasticity. *Brain Structure & Function* 223(9), pp. 1–15. [PubMed: 29222724]
- Han X, Chen M, Wang F, Windrem M, Wang S, Shanz S, Xu Q, Oberheim NA, Bekar L, Betstadt S, Silva AJ, Takano T, Goldman SA and Nedergaard M 2013 Forebrain engraftment by human glial progenitor cells enhances synaptic plasticity and learning in adult mice. *Cell Stem Cell* 12(3), pp. 342–353. [PubMed: 23472873]
- Harris KM, Jensen FE and Tsao B 1992 Three-dimensional structure of dendritic spines and synapses in rat hippocampus (CA1) at postnatal day 15 and adult ages: implications for the maturation of synaptic physiology and long-term potentiation. *The Journal of Neuroscience* 12(7), pp. 2685–2705. [PubMed: 1613552]
- Hayashi Y and Majewska AK 2005 Dendritic spine geometry: functional implication and regulation. *Neuron* 46(4), pp. 529–532. [PubMed: 15944122]
- Hering H and Sheng M 2001 Dendritic spines: structure, dynamics and regulation. *Nature Reviews. Neuroscience* 2(12), pp. 880–888. [PubMed: 11733795]

- Holtmaat A and Svoboda K 2009 Experience-dependent structural synaptic plasticity in the mammalian brain. *Nature Reviews. Neuroscience* 10(9), pp. 647–658. [PubMed: 19693029]
- Imura A, Iwano A, Tohyama O, Tsuji Y, Nozaki K, Hashimoto N, Fujimori T and Nabeshima Y-I 2004 Secreted Klotho protein in sera and CSF: implication for post-translational cleavage in release of Klotho protein from cell membrane. *FEBS Letters* 565(1–3), pp. 143–147. [PubMed: 15135068]
- Kaksonen M, Pavlov I, Vöikar V, Lauri SE, Hienola A, Riekkö R, Lakso M, Taira T and Rauvala H 2002 Syndecan-3-deficient mice exhibit enhanced LTP and impaired hippocampus-dependent memory. *Molecular and Cellular Neurosciences* 21(1), pp. 158–172. [PubMed: 12359158]
- Kasai H, Fukuda M, Watanabe S, Hayashi-Takagi A and Noguchi J 2010 Structural dynamics of dendritic spines in memory and cognition. *Trends in Neurosciences* 33(3), pp. 121–129. [PubMed: 20138375]
- Kasai H, Matsuzaki M, Noguchi J, Yasumatsu N and Nakahara H 2003 Structure-stability-function relationships of dendritic spines. *Trends in Neurosciences* 26(7), pp. 360–368. [PubMed: 12850432]
- Kim M-H, Choi J, Yang J, Chung W, Kim J-H, Paik SK, Kim K, Han S, Won H, Bae Y-S, Cho S-H, Seo J, Bae YC, Choi S-Y and Kim E 2009 Enhanced NMDA receptor-mediated synaptic transmission, enhanced long-term potentiation, and impaired learning and memory in mice lacking IRSp53. *The Journal of Neuroscience* 29(5), pp. 1586–1595. [PubMed: 19193906]
- King GD, Rosene DL and Abraham CR 2012 Promoter methylation and age-related downregulation of Klotho in rhesus monkey. *Age* 34(6), pp. 1405–1419. [PubMed: 21922250]
- Koyama D, Sato Y, Aizawa M, Maki T, Kurosawa M, Kuro-o M and Furukawa Y 2015 Soluble α Klotho as a candidate for the biomarker of aging. *Biochemical and Biophysical Research Communications* 467(4), pp. 1019–1025. [PubMed: 26462468]
- Krick S, Grabner A, Baumlin N, Yanucil C, Helton S, Grosche A, Sailland J, Geraghty P, Viera L, Russell DW, Wells JM, Xu X, Gaggari A, Barnes J, King GD, Campos M, Faul C and Salathe M 2018 Fibroblast growth factor 23 and Klotho contribute to airway inflammation. *The European Respiratory Journal* 52(1).
- Kunert SK, Hartmann H, Haffner D and Leifheit-Nestler M 2017 Klotho and fibroblast growth factor 23 in cerebrospinal fluid in children. *Journal of Bone and Mineral Metabolism* 35(2), pp. 215–226. [PubMed: 27017221]
- Kuro-o M, Matsumura Y, Aizawa H, Kawaguchi H, Suga T, Utsugi T, Ohyama Y, Kurabayashi M, Kaname T, Kume E, Iwasaki H, Iida A, Shiraki-Iida T, Nishikawa S, Nagai R and Nabeshima YI 1997 Mutation of the mouse klotho gene leads to a syndrome resembling ageing. *Nature* 390(6655), pp. 45–51. [PubMed: 9363890]
- Laszczyk AM, Fox-Quick S, Vo HT, Nettles D, Pugh PC, Overstreet-Wadiche L and King GD 2017 Klotho regulates postnatal neurogenesis and protects against age-related spatial memory loss. *Neurobiology of Aging* 59, pp. 41–54. [PubMed: 28837861]
- Lee Y-S and Silva AJ 2009 The molecular and cellular biology of enhanced cognition. *Nature Reviews. Neuroscience* 10(2), pp. 126–140. [PubMed: 19153576]
- Leon J, Moreno AJ, Garay BI, Chalkley RJ, Burlingame AL, Wang D and Dubal DB 2017 Peripheral Elevation of a Klotho Fragment Enhances Brain Function and Resilience in Young, Aging, and α -Synuclein Transgenic Mice. *Cell reports* 20(6), pp. 1360–1371. [PubMed: 28793260]
- Li Q, Vo HT, Wang J, Fox-Quick S, Dobrunz LE and King GD 2017 Klotho regulates CA1 hippocampal synaptic plasticity. *Neuroscience* 347, pp. 123–133. [PubMed: 28215989]
- Li S-A, Watanabe M, Yamada H, Nagai A, Kinuta M and Takei K 2004 Immunohistochemical localization of Klotho protein in brain, kidney, and reproductive organs of mice. *Cell Structure and Function* 29(4), pp. 91–99. [PubMed: 15665504]
- Lim SW, Jin L, Luo K, Jin J, Shin YJ, Hong SY and Yang CW 2017 Klotho enhances FoxO3-mediated manganese superoxide dismutase expression by negatively regulating PI3K/AKT pathway during tacrolimus-induced oxidative stress. *Cell death & disease* 8(8), p. e2972. [PubMed: 28771227]
- Löscher W, Hönack D, Fassbender CP and Nolting B 1991 The role of technical, biological and pharmacological factors in the laboratory evaluation of anticonvulsant drugs. III. Pentylentetrazole seizure models. *Epilepsy Research* 8(3), pp. 171–189. [PubMed: 1907909]

- Löscher W and Nolting B 1991 The role of technical, biological and pharmacological factors in the laboratory evaluation of anticonvulsant drugs. IV. Protective indices. *Epilepsy Research* 9(1), pp. 1–10. [PubMed: 1884714]
- Lu C, Chen Q, Zhou T, Bozic D, Fu Z, Pan JQ and Feng G 2016 Micro-electrode array recordings reveal reductions in both excitation and inhibition in cultured cortical neuron networks lacking Shank3. *Molecular Psychiatry* 21(2), pp. 159–168. [PubMed: 26598066]
- Lu T, Pan Y, Kao S-Y, Li C, Kohane I, Chan J and Yankner BA 2004 Gene regulation and DNA damage in the ageing human brain. *Nature* 429(6994), pp. 883–891. [PubMed: 15190254]
- Lu YM, Jia Z, Janus C, Henderson JT, Gerlai R, Wojtowicz JM and Roder JC 1997 Mice lacking metabotropic glutamate receptor 5 show impaired learning and reduced CA1 long-term potentiation (LTP) but normal CA3 LTP. *The Journal of Neuroscience* 17(13), pp. 5196–5205. [PubMed: 9185557]
- Maltare A, Nietz AK, Laszczyk AM, Dunn TS, Ballestas ME, Accavitti-Loper MA and King GD 2014 Development and characterization of monoclonal antibodies to detect klotho. *Monoclonal antibodies in immunodiagnosis and immunotherapy* 33(6), pp. 420–427. [PubMed: 25513981]
- Massó A, Sánchez A, Bosch A, Giménez-Llort L and Chillón M 2017 Secreted α Klotho isoform protects against age-dependent memory deficits. *Molecular Psychiatry*.
- Massó A, Sánchez A, Gimenez-Llort L, Lizcano JM, Cañete M, García B, Torres-Lista V, Puig M, Bosch A and Chillón M 2015 Secreted and Transmembrane α Klotho Isoforms Have Different Spatio-Temporal Profiles in the Brain during Aging and Alzheimer's Disease Progression. *Plos One* 10(11), p. e0143623. [PubMed: 26599613]
- Matsumura Y, Aizawa H, Shiraki-Iida T, Nagai R, Kuro-o M and Nabeshima Y 1998 Identification of the human klotho gene and its two transcripts encoding membrane and secreted klotho protein. *Biochemical and Biophysical Research Communications* 242(3), pp. 626–630. [PubMed: 9464267]
- Matsuzaki M, Ellis-Davies GC, Nemoto T, Miyashita Y, Iino M and Kasai H 2001 Dendritic spine geometry is critical for AMPA receptor expression in hippocampal CA1 pyramidal neurons. *Nature Neuroscience* 4(11), pp. 1086–1092. [PubMed: 11687814]
- Mattison HA, Popovkina D, Kao JPY and Thompson SM 2014 The role of glutamate in the morphological and physiological development of dendritic spines. *The European Journal of Neuroscience* 39(11), pp. 1761–1770. [PubMed: 24661419]
- McNaughton BL, Barnes CA, Rao G, Baldwin J and Rasmussen M 1986 Long-term enhancement of hippocampal synaptic transmission and the acquisition of spatial information. *The Journal of Neuroscience* 6(2), pp. 563–571. [PubMed: 3005525]
- Migaud M, Charlesworth P, Dempster M, Webster LC, Watabe AM, Makhinson M, He Y, Ramsay MF, Morris RG, Morrison JH, O'Dell TJ and Grant SG 1998 Enhanced long-term potentiation and impaired learning in mice with mutant postsynaptic density-95 protein. *Nature* 396(6710), pp. 433–439. [PubMed: 9853749]
- Moser EI, Krobot KA, Moser MB and Morris RG 1998 Impaired spatial learning after saturation of long-term potentiation. *Science* 281(5385), pp. 2038–2042. [PubMed: 9748165]
- Nagai T, Yamada K, Kim H-C, Kim Y-S, Noda Y, Imura A, Nabeshima Y and Nabeshima T 2003 Cognition impairment in the genetic model of aging klotho gene mutant mice: a role of oxidative stress. *The FASEB Journal* 17(1), pp. 50–52. [PubMed: 12475907]
- Niisato K, Fujikawa A, Komai S, Shintani T, Watanabe E, Sakaguchi G, Katsuura G, Manabe T and Noda M 2005 Age-dependent enhancement of hippocampal long-term potentiation and impairment of spatial learning through the Rho-associated kinase pathway in protein tyrosine phosphatase receptor type Z-deficient mice. *The Journal of Neuroscience* 25(5), pp. 1081–1088. [PubMed: 15689543]
- Page TL, Einstein M, Duan H, He Y, Flores T, Rolshud D, Erwin JM, Wearne SL, Morrison JH and Hof PR 2002 Morphological alterations in neurons forming corticocortical projections in the neocortex of aged Patas monkeys. *Neuroscience Letters* 317(1), pp. 37–41. [PubMed: 11750991]
- Van Pelt J, Wolters PS, Corner MA, Rutten WLC and Ramakers GJA 2004 Long-term characterization of firing dynamics of spontaneous bursts in cultured neural networks. *IEEE Transactions on Bio-Medical Engineering* 51(11), pp. 2051–2062. [PubMed: 15536907]

- Penn Y, Segal M and Moses E 2016 Network synchronization in hippocampal neurons. *Proceedings of the National Academy of Sciences of the United States of America* 113(12), pp. 3341–3346. [PubMed: 26961000]
- Pineda VV, Athos JI, Wang H, Celver J, Ippolito D, Boulay G, Birnbaumer L and Storm DR 2004 Removal of G(α 1) constraints on adenylyl cyclase in the hippocampus enhances LTP and impairs memory formation. *Neuron* 41(1), pp. 153–163. [PubMed: 14715142]
- Prather AA, Epel ES, Arenander J, Broestl L, Garay BI, Wang D and Dubal DB 2015 Longevity factor klotho and chronic psychological stress. *Translational psychiatry* 5, p. e585. [PubMed: 26080320]
- Roberson ED, Halabisky B, Yoo JW, Yao J, Chin J, Yan F, Wu T, Hamto P, Devidze N, Yu G-Q, Palop JJ, Noebels JL and Mucke L 2011 Amyloid- β /Fyn-induced synaptic, network, and cognitive impairments depend on tau levels in multiple mouse models of Alzheimer's disease. *The Journal of Neuroscience* 31(2), pp. 700–711. [PubMed: 21228179]
- Roberson ED, Scarce-Levie K, Palop JJ, Yan F, Cheng IH, Wu T, Gerstein H, Yu G-Q and Mucke L 2007 Reducing endogenous tau ameliorates amyloid beta-induced deficits in an Alzheimer's disease mouse model. *Science* 316(5825), pp. 750–754. [PubMed: 17478722]
- Rodriguez A, Ehlenberger DB, Dickstein DL, Hof PR and Wearne SL 2008 Automated three-dimensional detection and shape classification of dendritic spines from fluorescence microscopy images. *Plos One* 3(4), p. e1997. [PubMed: 18431482]
- Rutten K, Misner DL, Works M, Blokland A, Novak TJ, Santarelli L and Wallace TL 2008 Enhanced long-term potentiation and impaired learning in phosphodiesterase 4D-knockout (PDE4D) mice. *The European Journal of Neuroscience* 28(3), pp. 625–632. [PubMed: 18702734]
- Sarrouilhe D, di Tommaso A, Métyayé T and Ladeveze V 2006 Spinophilin: from partners to functions. *Biochimie* 88(9), pp. 1099–1113. [PubMed: 16737766]
- Saxe MD, Battaglia F, Wang J-W, Malleret G, David DJ, Monckton JE, Garcia ADR, Sofroniew MV, Kandel ER, Santarelli L, Hen R and Drew MR 2006 Ablation of hippocampal neurogenesis impairs contextual fear conditioning and synaptic plasticity in the dentate gyrus. *Proceedings of the National Academy of Sciences of the United States of America* 103(46), pp. 17501–17506. [PubMed: 17088541]
- Schneider CA, Rasband WS and Eliceiri KW 2012 NIH Image to ImageJ: 25 years of image analysis. *Nature Methods* 9(7), pp. 671–675. [PubMed: 22930834]
- Semba RD, Moghekar AR, Hu J, Sun K, Turner R, Ferrucci L and O'Brien R 2014 Klotho in the cerebrospinal fluid of adults with and without Alzheimer's disease. *Neuroscience Letters* 558, pp. 37–40. [PubMed: 24211693]
- Shiozaki M, Yoshimura K, Shibata M, Koike M, Matsuura N, Uchiyama Y and Gotow T 2008 Morphological and biochemical signs of age-related neurodegenerative changes in klotho mutant mice. *Neuroscience* 152(4), pp. 924–941. [PubMed: 18343589]
- Shiraki-Iida T, Aizawa H, Matsumura Y, Sekine S, Iida A, Anazawa H, Nagai R, Kuro-o M and Nabeshima Y 1998 Structure of the mouse klotho gene and its two transcripts encoding membrane and secreted protein. *FEBS Letters* 424(1–2), pp. 6–10. [PubMed: 9537505]
- Sun Q and Turrigiano GG 2011 PSD-95 and PSD-93 play critical but distinct roles in synaptic scaling up and down. *The Journal of Neuroscience* 31(18), pp. 6800–6808. [PubMed: 21543610]
- Swanger SA, Mattheyses AL, Gentry EG and Herskowitz JH 2015 ROCK1 and ROCK2 inhibition alters dendritic spine morphology in hippocampal neurons. *Cellular logistics* 5(4), p. e1133266. [PubMed: 27054047]
- Teocchi MA, Ferreira AÉD, da Luz de Oliveira EP, Tedeschi H and D'Souza-Li L 2013 Hippocampal gene expression dysregulation of Klotho, nuclear factor kappa B and tumor necrosis factor in temporal lobe epilepsy patients. *Journal of Neuroinflammation* 10, p. 53. [PubMed: 23634661]
- Uemura E 1980 Age-related changes in prefrontal cortex of *Macaca mulatta*: synaptic density. *Experimental Neurology* 69(1), pp. 164–172. [PubMed: 6771152]
- Uetani N, Kato K, Ogura H, Mizuno K, Kawano K, Mikoshiba K, Yakura H, Asano M and Iwakura Y 2000 Impaired learning with enhanced hippocampal long-term potentiation in PTPdelta-deficient mice. *The EMBO Journal* 19(12), pp. 2775–2785. [PubMed: 10856223]

- Vadakke Madathil S, Coe LM, Casu C and Sitara D 2014 Klotho deficiency disrupts hematopoietic stem cell development and erythropoiesis. *The American Journal of Pathology* 184(3), pp. 827–841. [PubMed: 24412515]
- Wang D, Cui Z, Zeng Q, Kuang H, Wang LP, Tsien JZ and Cao X 2009 Genetic enhancement of memory and long-term potentiation but not CA1 long-term depression in NR2B transgenic rats. *Plos One* 4(10), p. e7486. [PubMed: 19838302]
- Wong M and Guo D 2013 Dendritic spine pathology in epilepsy: cause or consequence? *Neuroscience* 251, pp. 141–150. [PubMed: 22522469]
- Xiao N, Zhang Y, Zheng Q and Gu J 2004 Klotho is a serum factor related to human aging. *Chinese Medical Journal* 117(5), pp. 742–747. [PubMed: 15161545]
- Xu B, Sun A, He Y, Qian F, Xi S, Long D and Chen Y 2018 Loss of thin spines and small synapses contributes to defective hippocampal function in aged mice. *Neurobiology of Aging* 71, pp. 91–104. [PubMed: 30118927]
- Xu X, Garcia J, Ewalt R, Nason S and Pozzo-Miller L 2017 The BDNF val-66-met Polymorphism Affects Neuronal Morphology and Synaptic Transmission in Cultured Hippocampal Neurons from Rett Syndrome Mice. *Frontiers in Cellular Neuroscience* 11, p. 203. [PubMed: 28751857]
- Xu X and Pozzo-Miller L 2017 EEA1 restores homeostatic synaptic plasticity in hippocampal neurons from Rett syndrome mice. *The Journal of Physiology* 595(16), pp. 5699–5712. [PubMed: 28621434]
- Yamazaki Y, Imura A, Urakawa I, Shimada T, Murakami J, Aono Y, Hasegawa H, Yamashita T, Nakatani K, Saito Y, Okamoto N, Kurumatani N, Namba N, Kitaoka T, Ozono K, Sakai T, Hataya H, Ichikawa S, Imel EA, Econs MJ and Nabeshima Y-I 2010 Establishment of sandwich ELISA for soluble alpha-Klotho measurement: Age-dependent change of soluble alpha-Klotho levels in healthy subjects. *Biochemical and Biophysical Research Communications* 398(3), pp. 513–518. [PubMed: 20599764]
- Yu Y, Li S, Zhang H, Zhang X, Guo D and Zhang J 2018 NRSF/REST levels are decreased in cholangiocellular carcinoma but not hepatocellular carcinoma compared with normal liver tissues: A tissue microarray study. *Oncology letters* 15(5), pp. 6592–6598. [PubMed: 29725406]
- Zhang H-M, Robinson N, Gómez-Curet I, Wang W and Harrington MA 2009 Neuronal and network activity in networks of cultured spinal motor neurons. *Neuroreport* 20(9), pp. 849–854. [PubMed: 19436229]
- Zito K, Scheuss V, Knott G, Hill T and Svoboda K 2009 Rapid functional maturation of nascent dendritic spines. *Neuron* 61(2), pp. 247–258. [PubMed: 19186167]

Highlights

Klotho deficiency causes spine morphology changes consistent with an increase in stable, mature dendritic spines.

Multi-electrode array recordings of klotho deficient neurons shows increased synchrony in burst firing.

Klotho deficient mice have a reduced latency to induced generalized seizure.

Klotho overexpression does not protect from seizure induction but does cause synaptic remodeling consistent with an increase in thin spines.

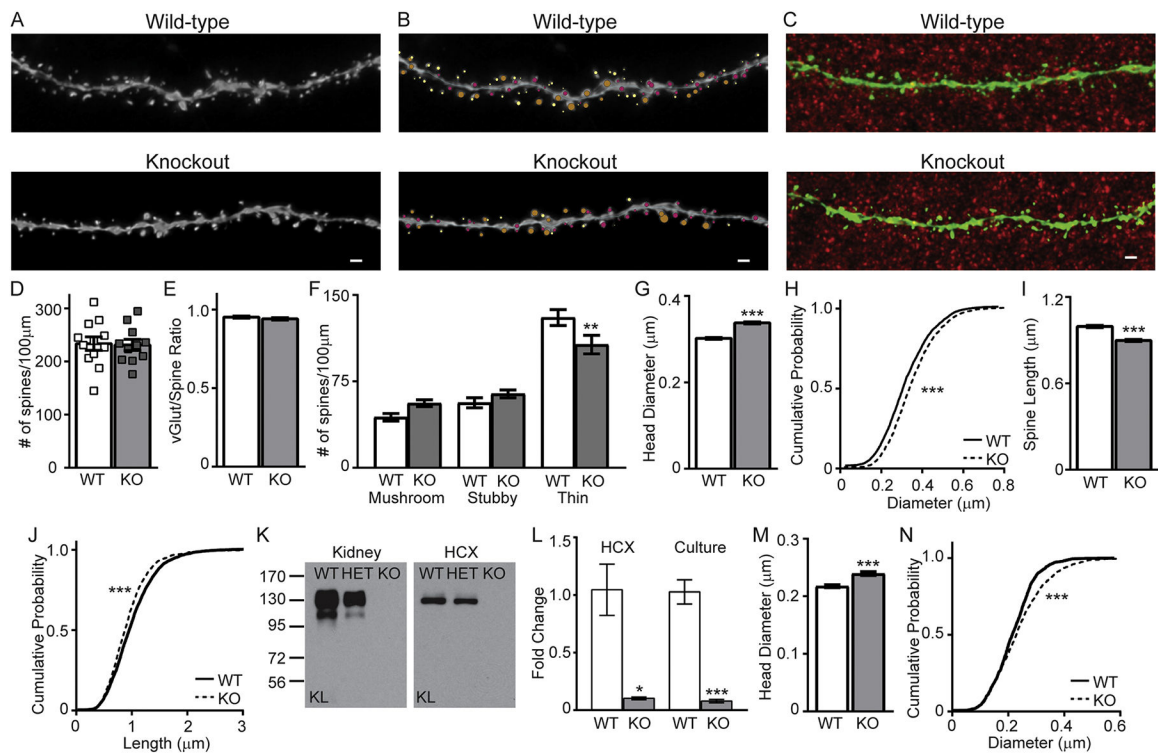


Figure 1 - Klotho deficiency causes changes to dendritic spine morphology.

A) Representative images of branches from apical dendrites of 7-week-old wild-type (WT; upper) and klotho-deficient (KO; lower) hippocampal CA1 neurons. Scale bar 1µm. **B)** Representative NeuronStudio reconstruction of WT (upper) and KO (lower): orange indicates mushroom spine, red indicates stubby spine, yellow indicates thin spine. Scale bar 1µm. **C)** Representative presynaptic vGlut (red) and post-synaptic spine (GFP, green) images from WT and KO neurons used for quantification of functional spines. **D)** Bar graph showing quantification of WT and KO average spine density (average number of spines/100µm of dendrite) overlaid with of each individual neuron's average spine density showing no change between groups. **E)** Quantification of the ratio of functional spines (the number of GFP+ post-synaptic spines with an apposing vGlut-immunolabeled presynapse) is not different between WT and KO. **F)** NeuronStudio classification of spine morphology shows fewer thin spines on KO neurons. **G,H)** The average KO spine head diameter is increased. Cumulative distribution of all spine head diameters shows a rightward shift in the KO (dashed line) curve consistent with a population of larger head spines. **I,J)** The average KO neuron spine length is decreased. Cumulative distribution of all spine lengths shows leftward shift in the KO curve consistent with shorter spine lengths across the population. (average \pm S.E.M.; $n=3$ brains/genotype; averaged measurements compared by Student's t-test or Mann-Whitney test where appropriate: ** $p<0.01$, *** $p<0.001$; cumulative probabilities compared by two-sample Kolmogorov-Smirnov test: *** $p<0.001$). **K)** Western blot validation of the KO model mouse kidney and hippocampus (HCX) with a dose-dependent deficiency of full-length KL expression (heterozygote: HET). **L)** qPCR validation of the KO mouse model and KL-deficient neuronal cultures. (average \pm S.E.M.; $n=3$ hippocampi or cultures/genotype; averaged measurements compared by Student's t-test: * $p<0.05$,

*** $p < 0.001$) **M,N**) The average spine head diameter of cultured KL KO neurons is increased relative to WT when measured either as the average spine head diameter or cumulative distribution of the population (average \pm S.E.M.; $n = 14$ WT neurons; 12 KO neurons; averaged measurements compared by Mann-Whitney test: *** $p < 0.001$; cumulative probability compared by two-sample Kolmogorov-Smirnov test: *** $p < 0.001$).

Author Manuscript

Author Manuscript

Author Manuscript

Author Manuscript

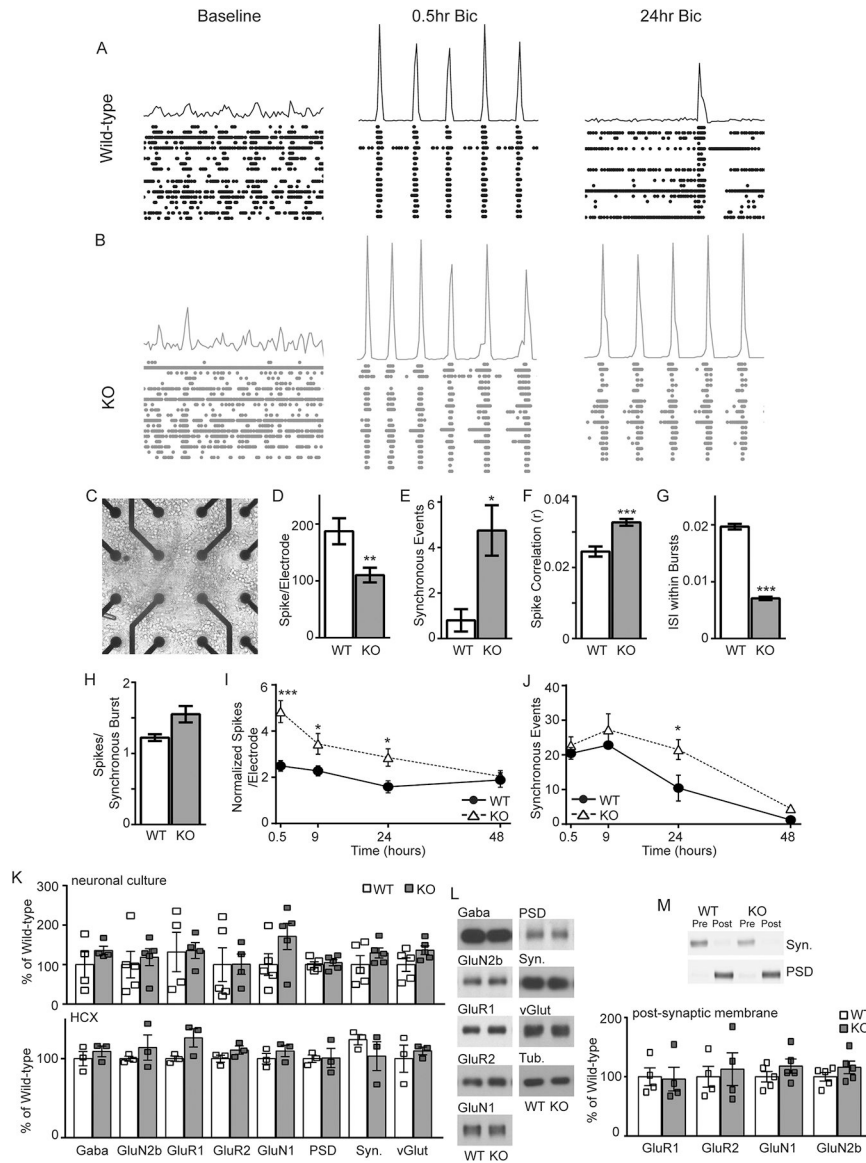


Figure 2 - Klotho deficiency regulates the activity of neurons cultured on multi-electrode arrays (MEAs).

A,B) Representative activity histograms showing activity from WT (wild-type, A) and KO (KL-deficient, B) neurons on MEAs at baseline (left), 0.5 hours with bicuculline (middle), and 24 hours with bicuculline (right). Bottom: raster plots of events across multiple electrodes. Note the difference in synchronous events at baseline and 24 hours with bicuculline. **C)** Representative image of neurons cultured on 60-electrode MEAs where each electrode is 30 μ m in diameter and separated by 200 μ m. **D)** Relative to WT, KO neurons average fewer spikes per electrode. **E)** Relative to WT, KO neurons average more synchronous events (2+ electrodes detecting simultaneous events). **F)** Relative to WT, KO neurons average an increased spike correlation (probability of simultaneous events occurring). **G)** Relative to WT, KO neurons average a decreased inter-spike interval (ISI) within bursts. **H)** WT and KO neurons show no change in the average number of spikes per burst. **I)** Upon bicuculline addition to media, KO neurons exhibit a sustained increase in

activity from 0.5 to 24 hours that is greater than WT neurons, as measured by the average number of spikes per electrode over time. **J**) Over time, synchronous WT and KO neuronal events demonstrate a homeostatic decrease in response to chronic increase of activity. Note that KO synchronous activity is increased at 24 hours with bicuculline indicating a delayed response to reduce activity. For details on statistical analysis from MEAs see the statistics section of Materials and Methods. Data graphed as average \pm S.E.M.; * $p < 0.05$, ** $p < 0.01$, *** $p < 0.001$. **K**) Quantification of band intensity normalized to β -tubulin expression and relevant WT control for neuronal culture lysates (upper) or total hippocampal lysates (HCX, lower). **L**) Representative Western blots from WT or KO mouse hippocampal lysates. Pre-synaptic markers: vGluT and synaptophysin (syn) and post-synaptic markers: GABA (GABA(A) $\alpha 1$ receptor), GluN2B, GluR1, GluR2, GluN1, PSD-95 (PSD), and loading control β -tubulin (tub). **M**) Representative Western blot of synaptic membrane separation (presynapse – Synaptophysin (syn), post-synapse PSD-95 (PSD) and quantification of ionotropic glutamate receptors from post-synaptic membranes. KO data normalized to loading control and WT. (Data graphed as average \pm S.E.M.; $n=3$ /genotype HCX, 4–5/genotype culture; $n=4$ –5/genotype synaptic membrane)

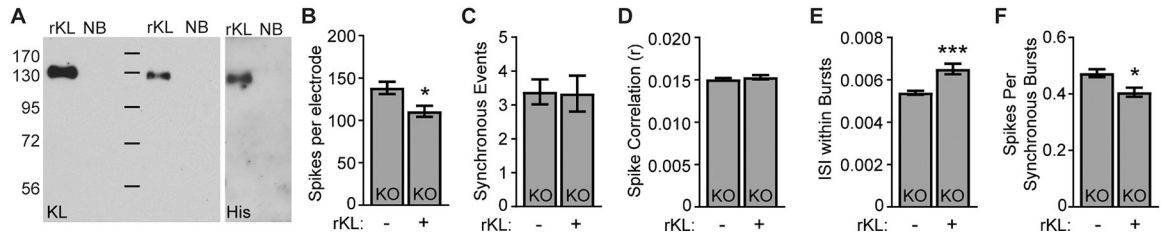


Figure 3 - Recombinant shed Klotho affects activity of cultured Klotho-deficient neurons.

A) Representative Western blot of recombinant shed KL (rKL) containing neurobasal media or neurobasal media alone (NB) detecting only one band at ~130kDa with either anti-klotho antibody (20 and 10ng shown) or anti-his tag antibody (20ng shown). **B)** Relative to untreated KO (KL-deficient) neurons, KO neurons supplemented with recombinant shed mouse KL (rKL) average fewer spike per electrode. However, no change in the average number of synchronous events (**C**) or spike correlation (**D**) occurred with rKL. Treatment of KO neurons with rKL increased average inter-spike interval within bursts (**E**) and reduced the number of spikes per burst (**F**). Statistical analysis from MEAs is detailed in the Materials and Methods. Data graphed as average \pm S.E.M.; * $p < 0.05$, *** $p < 0.001$.

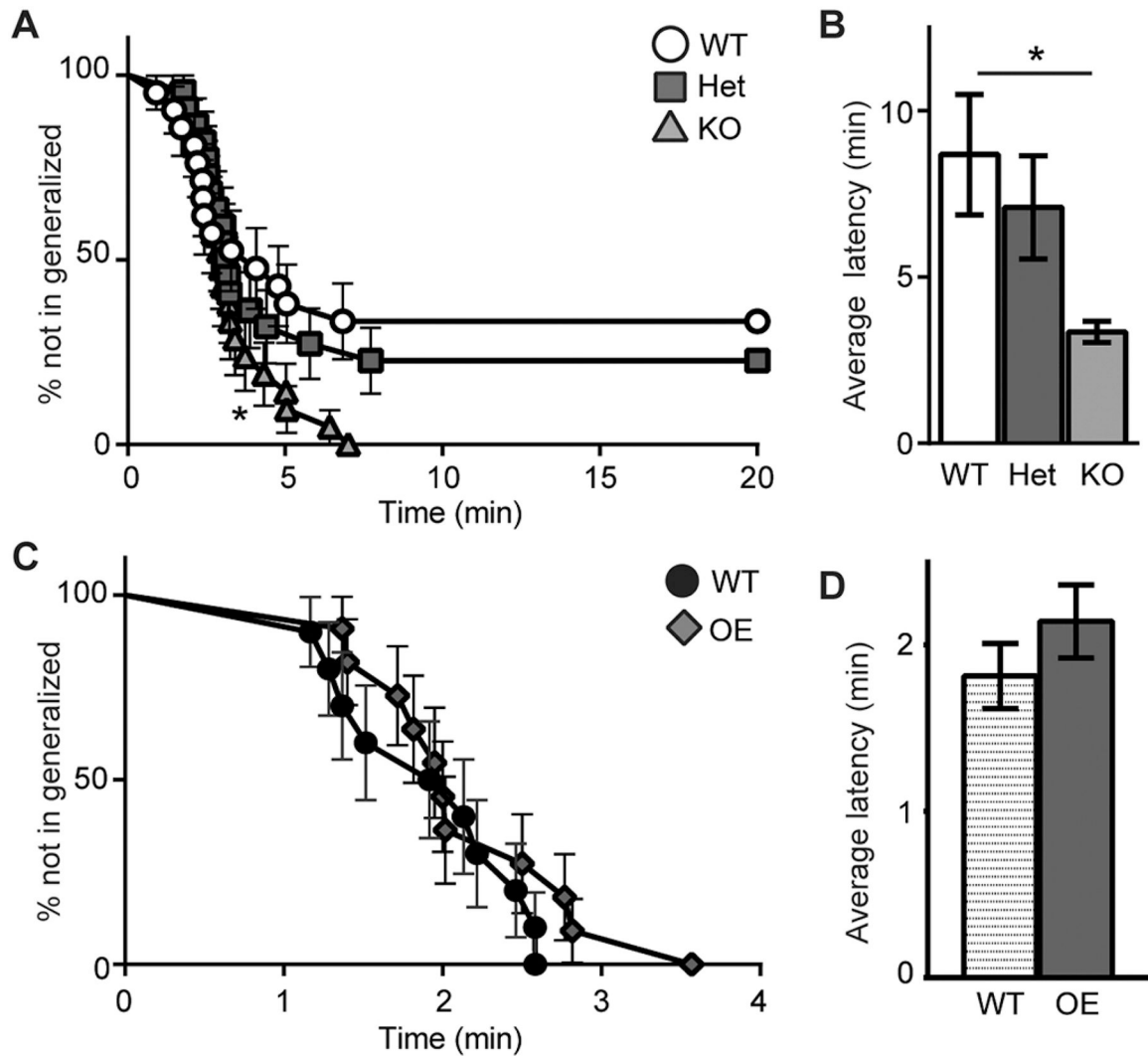


Figure 4 - Klotho-deficient mice show increased seizure susceptibility upon pentylenetetrazole challenge.

A) Latency to generalized tonic-clonic seizure (Stage 5) shown as the percent of all mice not at stage 5 at a given time (minutes). Unlike WT (wild-type) or KL-deficient heterozygote (Het) mice, all KO (KL-deficient) mice reached stage 5 within 20 minutes of a single PTZ injection. **B)** KO mice show a significantly decreased average latency to the generalized seizure stage (5-week-old mice, average \pm S.E.M.; $n=20$ WT; 21 HET, 20 KO, Logrank: $*p<0.03$ ANOVA: $*p<0.05$). **C, D)** In older C57BL6 wild-type (WT) and KL-overexpressing mice (OE), plotted either % of mice not in stage 5 at a given time or as the average latency, we measured no difference in latency to stage 5. (6–8-month-old mice, average \pm S.E.M.; $n=10$ WT; 11 OE; Logrank or t-test).

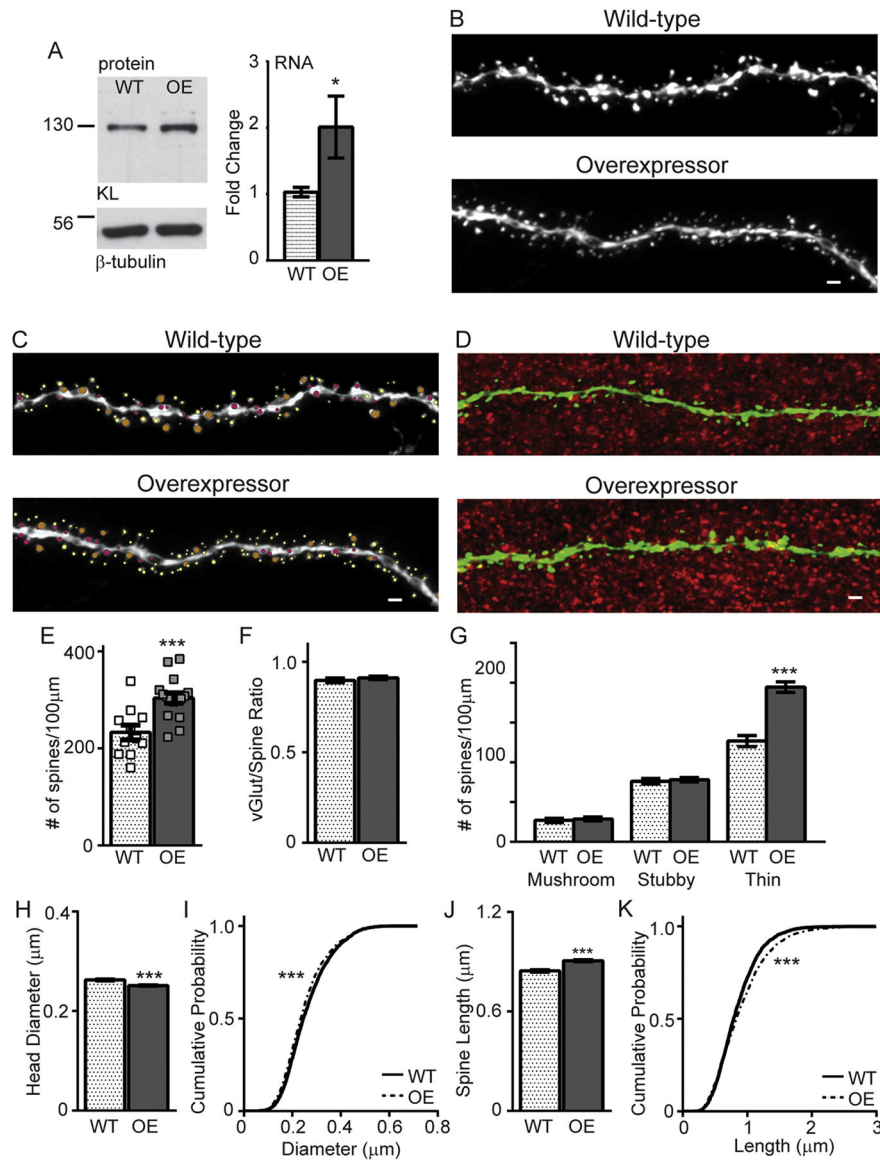


Figure 5 - Klotho-overexpressing mice show increased spine density and change to dendritic spine morphology.

A) Representative Western blot and qPCR validation of KL overexpression with the OE model mouse. **B)** Representative images from apical dendrites of 6-month-old wild-type (WT; upper) and KL-overexpressing (OE; lower) hippocampal CA1 neurons. Scale bar 1μm. **C)** Representative NeuronStudio reconstruction of WT (upper) and OE (lower): orange indicates mushroom spine, red indicates stubby spine, yellow indicates thin spine. Scale bar 1μm. **D)** Representative presynaptic vGlut (red) and post-synaptic spine (GFP, green) images from WT and OE neurons used for quantification of functional spines. **E)** Bar graph showing the quantification of WT and OE average spine density (average number of spines/100μm of dendrite) overlaid with each individual neuron's average spine density shows an increase in OE relative to age-matched WT. **F)** The ratio of functional spines measured by counting the number of GFP+ post-synaptic spines apposed to pre-synaptic vGlut puncta. No change was measured. **G)** NeuronStudio classification of spine morphology shows more OE thin spines

relative to WT. **H,I**) OE neurons show a decreased average spine head diameter. The population of spines reflects the decrease with a significant leftward shift in the population cumulative distribution of spine head diameters. **J,K**) The average OE neuron spine length is increased. Cumulative distribution of the population of spine lengths is increased as indicated by a rightward shift in the OE curve. (n=3 brains/genotype; averaged measurements compared with Student's t-test or Mann-Whitney test where appropriate: *** $p < 0.001$; cumulative probabilities compared by two-sample Kolmogorov-Smirnov test: *** $p < 0.001$).